Innovative Food Science and Emerging Technologies 104 (2025) 104134

Contents lists available at ScienceDirect

Innovative Food Science and Emerging Technologies

journal homepage: www.elsevier.com/locate/ifset

Non-invasive monitoring of goldenberry freezing using infrared thermography and radiofrequency dielectric spectroscopy

T. Chuquizuta [a,b], W. Castro [c], M. Castro-Giraldez [a,*], P.J. Fito [a]

[a] Instituto Universitario de Ingeniería de Alimentos FoodUPV, Universitat Politècnica de València, Camino de Vera s/n, Valencia 46022, Spain
[b] Instituto de Investigación del Mejoramiento Productivo, Universidad Nacional Autónoma de Chota, Chota 06120, Peru
[c] Facultad de Ingeniería de Industrias Alimentarias y Biotecnología, Universidad Nacional de Frontera, Sullana 20100, Peru

ARTICLE INFO

Keywords:
Infrared thermography
Radiofrequency
Spectrophotometry and freezing

ABSTRACT

This study presents a non-invasive monitoring system combining infrared thermography and radiofrequency dielectric spectroscopy to characterize the freezing behavior of goldenberry (*Physalis peruviana*). The system enabled simultaneous acquisition of surface temperature profiles, internal dielectric responses, and emissivity changes during freezing at −40 °C. Thermal imaging revealed distinct freezing stages, including subcooling, ice nucleation, and vitrification, with emissivity decreasing to 0.837 during initial dehydration and increasing to 0.951 near the glass transition (−35.8 °C). Emissivity variations revealed key thermal transitions, while dielectric measurements identified α- and β-dispersions linked to ionic straight and surface tension of ice Ih formation, with relaxation frequencies decreasing progressively as freezing advanced. The integration of both techniques allowed the detection of critical phase transitions, including the onset and completion of ice crystallization, supported by differential scanning calorimetry. These findings provide insight into structural changes and water mobility in high-moisture fruits, enabling real-time assessment of freezing kinetics. The approach demonstrates significant potential for optimizing industrial freezing protocols, improving the preservation of delicate fruits by minimizing structural damage and degradation of bioactive compounds.

1. Introduction

Goldenberry (*Physalis peruviana*) is an exotic fruit native to the Peruvian Andes, recognised for its nutritional value and its high content of bioactive compounds, such as carotenoids, polyphenols, flavonoids and vitamin C (Olivares-Tenorio, Dekker, Verkerk, & van Boekel, 2016; L. A. Puente, Pinto-Muñoz, Castro, & Cortés, 2011). A substantial body of research has demonstrated that these compounds possess antioxidant, anti-inflammatory, and immunomodulatory properties (L. Puente et al., 2021; L. A. Puente et al., 2011; Vasco, Ruales, & Kamal-Eldin, 2008). Notwithstanding its nutritional benefits and growing demand in the agri-food industry, goldenberry is considered a highly perishable fruit (Balaguera-López, Espinal-Ruiz, Zacarías, & Herrera, 2017; Lopez, Fischer, & Magnitskiy, 2024; Ozcelik, Ozcelik, Aksu, & Ozkan, 2024). This is attributed to its rapid postharvest metabolism and high enzymatic activity, which generates losses of mass, texture and bioactive compounds along the marketing chain. In this context, the implementation of effective preservation techniques is imperative to extend their shelf life and maintain their nutritional and sensory properties.

Freezing is one of the most commonly applied preservation methods for fruits, offering extended shelf life and minimal nutrient loss. This method involves subjecting the food to temperatures below 0 °C, which has been shown to reduce water mobility (intra- and extracellular) and water activity (a_w) (Chi Khang, Le Dang, Van Muoi, & Thanh Truc, 2022; Da Silva, Silveira, Ronzoni, & Hermes, 2022). This, in turn, has been demonstrated to decrease chemical reactions, as well as enzymatic and microbial activity (De Ancos, Sánchez-Moreno, De Pascual-Teresa, & Cano, 2012; Delgado & Sun, 2001; Loayza-Salazar et al., 2024). In this context, freezing has been shown to preserve the sensory quality (i.e. odour, colour and taste) and nutritional value of the product (Ojha, Kerry, Tiwari, & O'Donnell, 2016).

During the freezing process, the phenomena of heat and mass transfer are contingent on the properties of the foodstuff, including its composition, porosity, density and surface area (Delgado & Sun, 2001). Consequently, the freezing process can be categorized into three distinct stages: initial cooling, phase change (nucleation and ice formation), and tempering. The subsequent cooling stage involves the reduction of the initial temperature to the sub cooling temperature, below the freezing

* Corresponding author.
E-mail address: marcasgi@upv.es (M. Castro-Giraldez).

https://doi.org/10.1016/j.ifset.2025.104134
Received 13 June 2025; Received in revised form 18 July 2025; Accepted 28 July 2025
Available online 28 July 2025

point, where the nucleation is produced. The phase change stage is characterized by the initiation of nucleation and the subsequent growth of ice crystals, a consequence of the surface tension of water ice Ih, and its state transition (liquid – solid). Finally, the tempering stage begins after the completion of the phase change and concludes when thermal equilibrium is established between the sample and the ambient freezing conditions (Ben Haj Said, Bellagha, & Allaf, 2016; De Ancos et al., 2012; Tomas-Egea, Castro-Giraldez, Colom, & Fito, 2022). However, the efficiency of the freezing process is closely related to a number of phenomena, including the kinetics of formation and agglomeration of ice crystals of the type Ih, as well as the vitrification processes undergone by the fruit. Among these critical phenomena are sub cooling, the initial freezing point (T_{m0}), the freezing temperature of the maximally cryo-concentrated sample (T_m') and the glass transition temperature (T_g') of the sample. These phenomena are instrumental in determining the structural and biochemical stability of the product during frozen storage (Fan & Roos, 2017; Roos, 1993; Talja & Roos, 2001). In view of this, the monitoring of ice formation in food is of utmost importance, as is the determination of technical parameters such as those mentioned above, which are to be transferred to the industry dedicated to freezing processes of exotic fruits, due to the paucity of research in this area.

The present study investigates the monitoring of ice formation in plant tissues using thermocouples. Despite their accuracy and low measurement error, these techniques are destructive due to their insertion into the food tissue (surface and/or center), causing damage to the structure (cells), leakage of intra- and extra-cellular liquid, and contamination of the samples (Cuibus, Castro-Giraldez, Fito, & Fabbri, 2014; Li, Cheng, & Cheng, 2025). Consequently, the frozen fruit industry (predominantly the goldenberry industry) has been demanding novel non-invasive methods to monitor the surface temperature of the food.

Infrared thermography technology (deriving from infrared radiation) constitutes a component of thermal analysis methods, with a focus on the acquisition and processing of thermal images (Gonçalves et al., 2018; Usamentiaga et al., 2014). This technique has been shown to have several advantages, including being non-invasive, fast and objective for the analysis of non-contact surface temperature profiles (Gonçalves, Giarola, Pereira, Vilas Boas, & de Resende, 2016; Harrap, Hempel de Ibarra, Whitney, & Rands, 2018; Shammi et al., 2022). Recent advances in the field have also explored the integration of thermal imaging and spectroscopic techniques to characterize internal structural heterogeneity and firmness distribution in fruits (Lan et al., 2024; Wang et al., 2024), supporting the relevance of advanced non-invasive tools for assessing quality attributes in plant-based systems. In recent years, there has been a concerted effort to apply infrared thermography to a variety of contexts. For instance, Gonçalves et al. (2018) have used the technique to monitor the heat transfer process during the freeze-drying of gelatin solutions with ethanol, while Shammi et al. (2022); Shammi, Sohel, Diepeveen, Zander, and Jones (2023) have employed infrared thermography to detect frost in crops. In the following years, research has been conducted on the estimation of freeze-dryer plate temperature (Li et al., 2025), the detection of water stress in almond plants (Poirier-Pocovi, Volder, & Bailey, 2020), the analysis of heat stress in insects (Gallego, Verdú, Carrascal, & Lobo, 2016) and the assessment of lesions in cold-stored guava (Gonçalves et al., 2016). The extant literature demonstrates the potential of using thermal imaging cameras in agricultural and biological applications. However, the majority of these investigations do not consider the determination of emissivity and do not make corrections to accurately estimate the real temperature of the object under study.

In this context, the determination of the emissivity of a body from its radiant energy becomes relevant, considering that the thermal camera sensor captures not only the energy emitted by the object under study, but also the energy of the surrounding air and the radiation reflected from the environment (Usamentiaga et al., 2014). A paucity of studies has been identified that address the determination and/or correction of object emissivity in agri-food processes. The following studies are notable in this respect: the drying of pork (Traffano-Schiffo, Castro-Giraldez, Fito, & Balaguer, 2014); the drying of potatoes (Tomas-Egea, Traffano-Schiffo, Castro-Giraldez, & Fito, 2021); the freezing of pork (Castro-Giraldez, Balaguer, Hinarejos, & Fito, 2014); and the freezing of potatoes (Cuibus et al., 2014). However, research applying infrared thermography to small and structurally complex fruits such as goldenberry has not yet been reported.

Spectrophotometry is a technique based on the interaction of photons with matter along the electromagnetic spectrum, the behavior of which can be modelled from quantum theory via the Schrödinger equation (Chandra Roychoudhuri, 2017). At the macroscopic level, Maxwell's equations facilitate the description of the interaction between electric and magnetic fields and materials, represented respectively through the complex permittivity and the material complex permeability (Tomas-Egea et al., 2022; Traffano-Schiffo, Castro-Giraldez, Colom, & Fito, 2018; Traffano-Schiffo, Castro-Giraldez, Colom, Talens, & Fito, 2021). Permittivity is a vectorial property consisting of a real part (ε'), which is associated with the material's capacity to store electrical energy, and an imaginary part (ε″), which is related to dielectric losses. Within the radiofrequency range, the dielectric behavior facilitates the identification of three primary contributions across the spectrum: two associated with molecular orientation effects (α and β dispersions), and one linked to molecular vibration and ionic conduction (σ) (Heileman, Daoud, & Tabrizian, 2013; Kuang & Nelson, 1998; Liu & Guo, 2017). The α- dispersions (Hz-kHz range) has been shown to be associated with charged molecules that exhibit low mobility and high ionic strength, such as electrolytes and organic acids. Conversely, β-dispersions (kHz-MHz) has been observed to be associated with charged macromolecules, such as proteins and carbohydrates, in addition to interactions at interfacial surfaces that exhibit charges with high surface tension (Cuibus et al., 2014; Tomas-Egea et al., 2022; Traffano-Schiffo et al., 2018, 2021).

Recent studies have demonstrated that dielectric analysis (α- and β-dispersions) can detect changes in molecular structure associated with the glass transition (T_g'), thus providing a non-destructive tool for monitoring product stability during the freezing process (Fan & Roos, 2017; Tomas-Egea et al., 2022). Despite the advances in the individual use of these technologies, their joint application to monitor and understand freezing processes in fruits such as goldenberry remains limited. The integration of infrared thermography and radiofrequency spectrophotometry has the potential to provide a more comprehensive understanding of thermal and dielectric events during the freezing process. This, in turn, could facilitate a more precise characterization of physical transitions, thereby contributing to the development of enhanced preservation protocols.

2. Materials and methods

The experimental procedure is shown in Fig. 1. Likewise, each step of the flowchart is explained in the following paragraphs.

2.1. Sample goldenberry fruits

The samples of fresh goldenberry fruit at commercial ripeness, coming from Ecuador, were obtained through the importing company Ammarket (Orihuela, Alicante - Spain). The goldenberry fruits arrived in refrigerated boxes (100 g / box) with uniform size (diameter) and weight, 3.8 ± 0.21 cm and 3.9 ± 0.4 g, respectively, which were kept in a refrigerator at 6 °C until later analysis and execution of the experiment.

2.1.1. Soluble solids content

The soluble solids (°Brix) of the goldenberry juice were determined using the AOAC method 932. This involved placing 3 to 5 drops of the juice on the lens of the Hanna HI96800 refractometer and taking a reading.

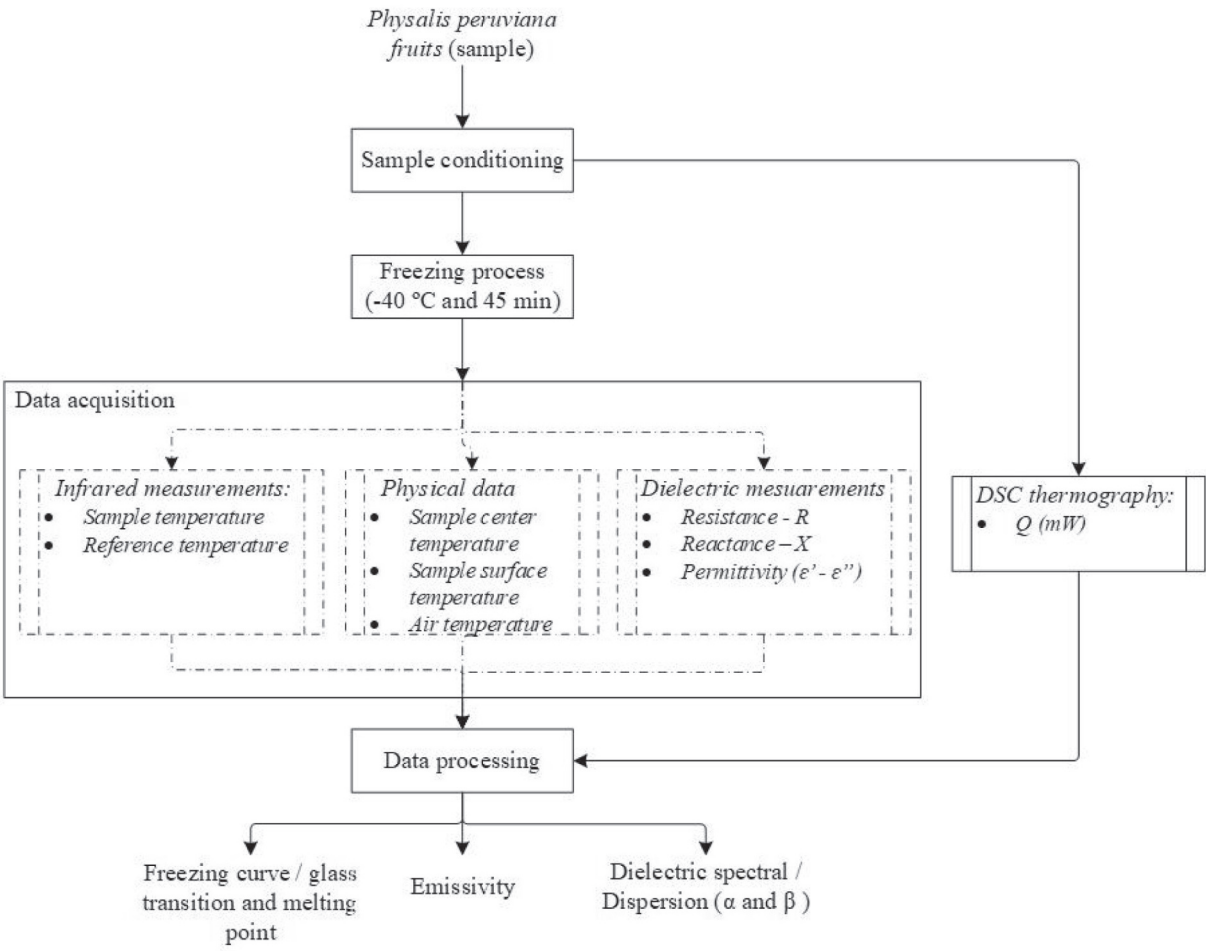

Fig. 1. Experimental procedure in freezing process of *Physalis peruviana*.

2.1.2. Moisture

The fruit's moisture (in dry basis) was characterized using the methodology of AOAC Method 934.06, 2000.

2.2. Sample conditioning

Prior to the experiment, the goldenberry fruits were removed from

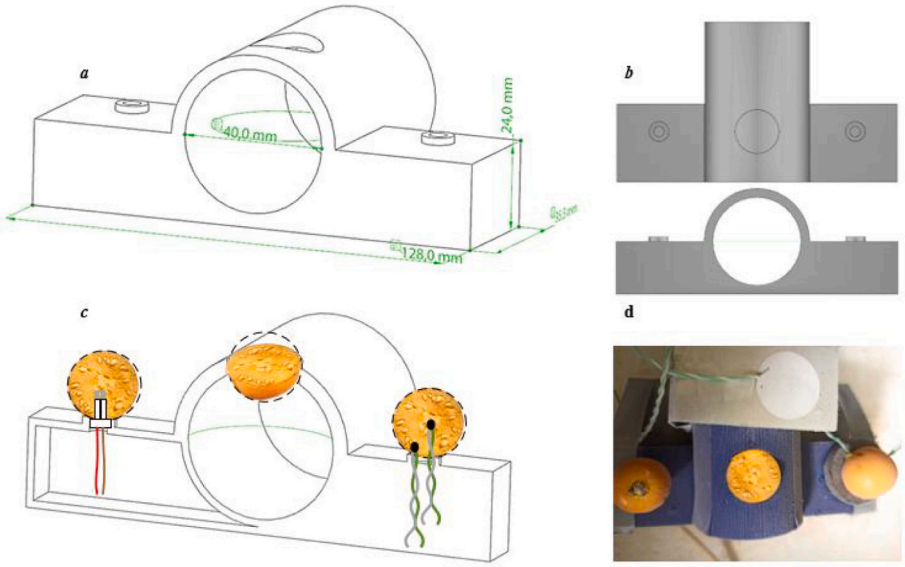

Fig. 2. Sample conditioning by sample holder: a) Isometric drawing of the sample holder; b) top and side views of the sample holder; c) location of the samples for the extraction of information (temperature and dielectric properties) and d) conditioning of the fruit in the holder.

the refrigerator and acclimatized at room temperature (18.5 ± 0.6 °C) for a period of 24 h. Furthermore, a sample holder was designed and printed in PLA) with a 3D printer to facilitate the monitoring of the freezing process of the fruits (Fig. 2). The order in which the fruits were placed in the sample holder was as follows: on the right side, the first fruit was used for temperature monitoring using K-type thermocouples (surface and center); in the center, the second fruit was used for surface temperature monitoring using an infrared camera; and on the left side, the third fruit was used for the measurement of dielectric properties.

2.3. Freezing process

In the present study, data acquisition systems were installed for the purpose of monitoring the freezing process of godenberry fruit. This work is founded upon the contributions of Tomas-Egea et al. (2022) and Cuibus et al. (2014) the installation of the systems involved the measurement of surface and core temperature of the sample, surface temperature by thermographic camera, and dielectric properties (Fig. 2). Prior to the initiation of the freezing process, the sample holder was positioned on an expanded polystyrene box, which was then situated in the center of a horizontal convective air freezer (model ACR-45/87, Dycometal, SL, Barcelona, Spain), with no-frost technology. This configuration ensured that the forced cold airflow would directly contact the fruit (Figs. 2, b and d). This approach facilitated effective convective heat transfer from the air to the fruit, as well as radial conduction heat transfer (from the surface to the center) within the fruit.

In addition, three goldenberry fruits were utilized in each experiment, positioned within the designated sample holder (Fig. 2, c). The initial fruit was positioned on the right, with the objective of conducting temperature monitoring (both surface and core) through the utilization of two K-type thermocouples, with data recorded at an interval of 5 s. The temperature was recorded using an Agilent 34972 A data acquisition system (Agilent Technologies, Malaysia). Additionally, the surface temperature of the 25 mm diameter certified emissivity reference material (ε = 0.95) (Optris GmbH, Berlin, Germany) and the air temperature inside the freezer were monitored. The second fruit was positioned centrally for measuring surface temperature. This was accomplished by means of a thermographic camera (Optris PI® 160, Optris GmbH, Berlin, Germany) positioned at a distance of 30 cm, with recordings being conducted at an interval of 0.5 s. The camera was connected directly to a laptop (PCG - 2L5M, Sony WAIO, USA) for the purpose of recording frames (video) of the goldenberry fruit and emissivity reference material during the online freezing process. The third fruit was positioned on the left, with the objective of monitoring the dielectric properties by means of a two-needle sensor that was inserted in the center of the sample. This was connected to an Agilent 4294 A impedance analyzer (Agilent Technologies, Santa Clara, CA, USA).

Following the installation of the data acquisition systems and the placement of the goldenberry fruits in the sample holder, an extruded polystyrene sheet (Chovafoam type 4I, Leroy Merlin SL, Valencia, Spain) was utilized as thermal insulation. The sheet, measuring 68 cm × 52 cm × 3 cm, was utilized as the lid of the chest freezer and was affixed with adhesive tape to minimize heat ingress from the external environment. Furthermore, the apparatus featured a central aperture measuring 7 cm in diameter, which served as the site for the integration of the thermographic camera. The freezing process of the goldenberry fruits was conducted at a temperature of −40 °C for a duration of 45 min, with an air flow of 1 m/s, within a horizontal freezer equipped with forced air ventilation (model ACR-45/87, Dycometal, SL, Barcelona, Spain) (Fig. 3).

2.4. Infrared thermography

According to Tomas-Egea et al. (2022) and Traffano-Schiffo et al. (2014), in order to obtain thermal images, the thermal camera operates under the following conditions: two-dimensional focal plane (matrix) of 160 × 120 pixels, spectral range of 7.5–13.0 μm, resolution of 0.05 °C and accuracy of ±2 %. The thermal camera measures in a temperature range of −20 to 900 °C, with a field of view (FOV) of 23° x 17° at a minimum distance of 20 mm and a frame rate of 120 Hz, which is

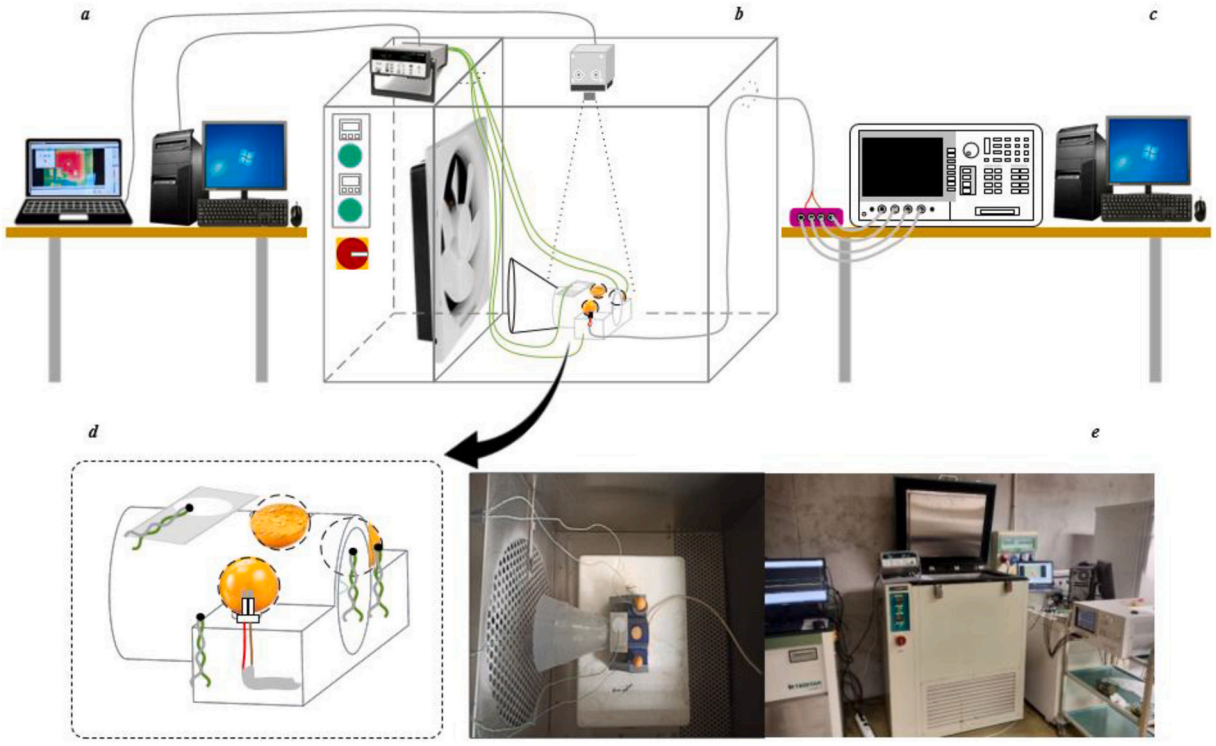

Fig. 3. The freezing process monitoring system is comprised of the following components: a) Thermal data acquisition; b) Freezing process; c) Dielectric data acquisition; d) Sample holder and e) Real environment.

connected to a desktop computer to record thermal images throughout the freezing process using the Optris PI Connect software (Optris GmbH, Berlin, Germany). Similarly, the reference emissivity material (radius = 12.5 mm and ε = 0.95) was placed parallel to the lens of the thermographic camera at a distance of 30 cm to calculate the reflected energy received by the thermographic camera (Fig. 3, b).

2.5. Dielectric properties

The dielectric properties of the goldenberry were obtained by means of a needle-type dielectric sensor, taking as a reference the work carried out by Tomas-Egea et al. (2022). The dielectric sensor is composed of two steel needles, the dimensions of which are as follows: The dimensions of the perforation are recorded as 1 mm diameter, 2 mm height and 1.5 mm separation between them (Fig. 4). The perforation penetrates the lower part of the fruit (perpendicular to the equatorial line) until reaching the center (see Fig. 2c). The dielectric sensor was connected to a 4294 A impedance analyzer (Agilent Technologies, Santa Clara, CA, USA), which was operated remotely via a desktop computer (ThinkCentre Type 7099 - 7099B8G, Lenovo, China), allowing online monitoring.

Prior to the calibration of the impedance analyzer, it was required to stabilize for a minimum of one hour in order to eliminate possible static charges or stray current (Chuquizuta et al., 2022; Guo, Fang, Liu, & Wang, 2015; Liu & Guo, 2017). The calibration was conducted in accordance with the open-air and short-circuit methodologies outlined by Tomas-Egea et al. (2022). The values of the complex impedance spectrum (resistance - R and reactance - X) were measured in the frequency (*f*) range (40 Hz to 1 MHz), with 401 data points obtained. The impedance values thus obtained permitted the calculation of dielectric properties using Eqs. 1, 2 and 3 (Traffano-Schiffo et al., 2018).

$$C_0 = \frac{\varepsilon_0 S}{d} \tag{1}$$

$$\varepsilon' = \frac{-X}{(R^2 + X^2)} \quad \frac{1}{2\pi f C_0 10^{-12}} \tag{2}$$

$$\varepsilon'' = \frac{R}{R^2 + X^2} \quad \frac{1}{2\pi f C_0 10^{-12}} \tag{3}$$

Where C_0 is the vacuum capacitance (pF), e_0 is the vacuum permittivity (C^2/Nm^2), S is the sensor poles surface (m^2), d is the distance between poles (m). In order to observe the influence of the freezing process on the fruit, as well as on its dielectric properties, it is necessary to obtain the α and β relaxations in the radiofrequency range. To this end, eqs. 4, 5, 6 and 7 proposed by Traffano-Schiffo et al. (2018) were utilized to ascertain the α and β relaxation parameters.

$$\log\epsilon'(\omega) = \log\epsilon'_\infty + \sum_{n=1}^{2} \frac{\Delta\log\epsilon'_n}{1 + e^{\left(\log\omega^2 - \log\tau_n^2\right)^* \alpha_n}} \tag{4}$$

Where *n* is given by the dispersions of α and β, $\log\epsilon'$represents the logarithm of the dielectric constant, $\log\epsilon'_\infty$ is the logarithm of the dielectric constant at high frequencies, $\log\omega$ is the logarithm of the angular frequency (rad/s) and Dloge'$_n$ is the amplitude of the dispersion n, $\log\tau_n$ is the logarithm of the angular frequency at relaxation time ($t_{rel} = 1/t_n$) for each dispersion, $\alpha_n$is the slope of the dispersion.

Also, from the parameters obtained from Eq. 4, the dielectric constant and the relaxation frequency for each of the dispersion in the radio frequency range have been calculated (Eq. 5, 6 and 7) (Traffano-Schiffo et al., 2018).

$$\epsilon'_\alpha = 10^{\left(\log\epsilon'_\infty + \Delta\log\epsilon'_\beta + \frac{\Delta\log\epsilon'_\alpha}{2}\right)} \tag{5}$$

$$\epsilon'_\beta = 10^{\left(\log\epsilon'_\infty + \frac{\Delta\log\epsilon'_\beta}{2}\right)} \tag{6}$$

$$f_i = 10^{\left(\frac{\log\omega_{ri}}{2^*\pi}\right)} \tag{7}$$

Where *i* corresponds to each dispersion (α and β).

2.6. Differential scanning calorimeter

The methodology proposed by Vega-Gálvez, López, Ah-Hen, Torres, and Lemus-Mondaca (2014), with slight modifications, was utilized to ascertain the glass transition temperature (T_g) and heat capacity (c_p) of fresh goldenberry samples. The thermal profiles of the samples were obtained using a differential scanning calorimeter (DSC, system 1 StarE, Mettler-Toledo, Switzerland), which was calibrated using the automatic calibration function FlexCal, as recommended by the manufacturer. Each sample (10 to 15 mg) was weighed directly onto a 40 μL DSC aluminum tray (Mettler Toledo, ME-00026763) using a Mettler Toledo XS-205 balance, without considering the mass of the tray. Subsequently, the tray was hermetically sealed in order to prevent any loss of moisture during the analysis. The sample trays, in conjunction with an empty tray that served as a control, were placed in the DSC oven. All experiments were performed in triplicate using the following thermal profile: samples were cooled from room temperature to −50 °C at a rate of −5 °C/

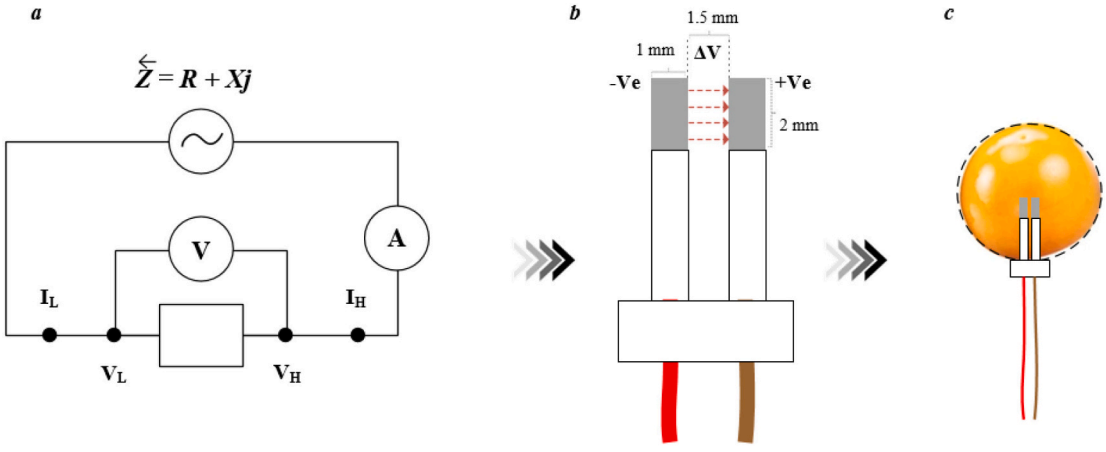

Fig. 4. Schematic representation of the experimental setup used to measure the dielectric properties at the center of the goldenberry sample during the freezing process. a) Electrical circuit diagram for impedance measurement; b) Sensor configuration showing the applied electric field; and c) Sensor positioning at the core of the fruit.

min, and held for 30 min to ensure complete freezing of the sample. Subsequently, the samples were subjected to a heating protocol, encompassing a temperature range from −50 °C to 80 °C at a constant heating rate of 10 °C/min. A maintenance period of one minute was implemented to ensure the stability of the temperature before proceeding to the subsequent stage of the experiment.

2.7. Statistic

The Levenberg-Marquardt algorithm, as implemented in the MATLAB 2024b software (MathWorks), was utilized to fit the data to the Traffano-Schiffo model and subsequently calculate the dielectric relaxations α and β. Furthermore, the implemented algorithm was constrained to a maximum of 400 interactions, with a convergence threshold set at 1×10^{-6}. For the purpose of statistical analysis, the coefficient of determination (R^2) and root mean square error (RMSE) were evaluated at the 95 % confidence level, with eqs. (8) and (9) being employed for this purpose.

Furthermore, a univariate analysis of variance (ANOVA) and a Tukey's post hoc test ($\alpha = 0.05$) were conducted on goldenberry heat capacity, utilising Statgraphics Centurion V.19 software.

$$R^2 = \frac{\sum_{i=1}^{n}(\hat{y}_i - y_i)^2}{\sum_{i=1}^{n}(\hat{y}_i - y_t)^2} \tag{8}$$

$$RMSE = \sqrt{\frac{1}{n}\sum_{i=1}^{n}(y_i - \hat{y}_i)^2} \tag{9}$$

Where, $\hat{y}_i$ is the experimental value, y_i is the predicted value and n is the number of observations.

3. Results

3.1. Freezing kinetics

Figure 5 shows the freezing curve pertaining to both the surface and center of the goldenberry that was obtained by means of K-type thermocouples over the course of a 45 min period. Three distinct stages were identified during the freezing process: After the initial cooling of the sample, a subcooling stage occurs, followed by a phase change (nucleation and freezing), and concluding with a tempering stage until thermal equilibrium with the freezing air is reached. During the cooling stage, a decrease in temperature was observed at the surface and in the center of the sample at different times. In the surface, the subcooling stage was reached at 3.3 ± 0.4 min and at −2.28 ± 0.03 °C, and in the center of the sample, this stage was reached at 7 ± 1 and − 1.93 ± 0.07 °C. This temperature difference is attributed to variations in the freezing rate, resulting from both convective and conductive heat transfer mechanisms (Guizani, Al-Saidi, Rahman, Bornaz, & Al-Alawi, 2010; Struchaiev, Postol, Stopin, & Borokhov, 2019). These effects are further influenced by changes in solute concentration during the freezing process, which lead to a progressive decrease in the freezing temperature and involve simultaneous variations in internal energy and phase change energy (Ben Haj Said et al., 2016; Hajji, Gliguem, Bellagha, & Allaf, 2022). Thus, marking the initiation of nucleation and the formation of ice crystals within the fruit tissue. During this period, most of the water solidifies, while the remaining liquid phase, primarily composed of non-electrolyte solutes, undergoes cryoconcentration, leading to a gradual decrease in the freezing temperature. In the subsequent phase, the supersaturated liquid phase induces a sudden drop in freezing temperature, and a tempering process in which the sample equilibrates with the temperature of the freezing air (Cuibus et al., 2014; Struchaiev et al., 2019). This decrease corresponds to the third stage of the process in which the sample reaches the thermal equilibrium with the air medium (Auleda, Raventós, Sánchez, & Hernández, 2011; Da Silva et al.,

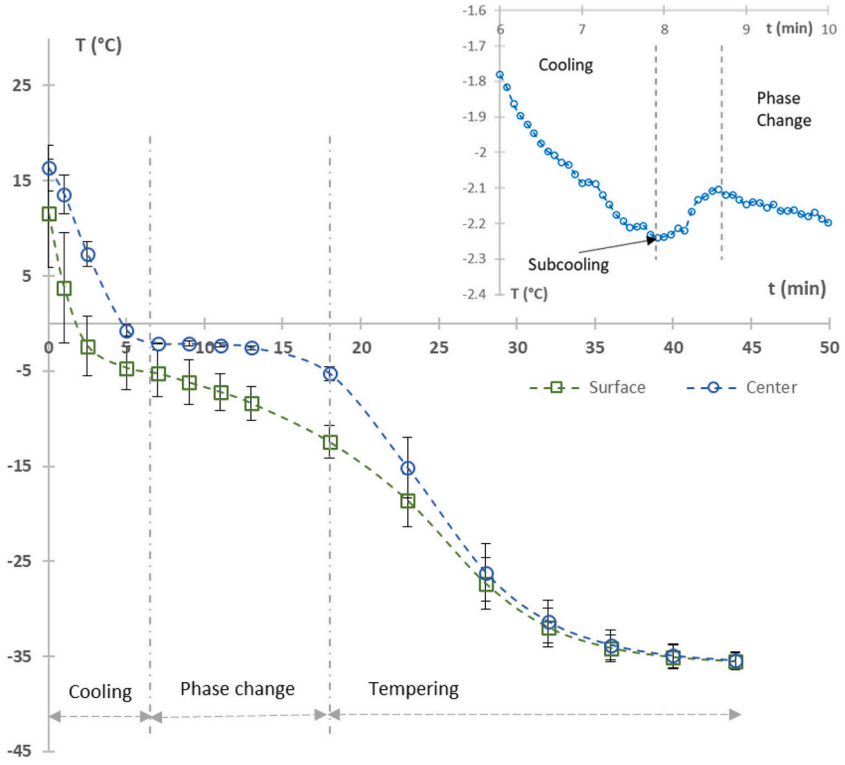

Fig. 5. Freezing curve of fresh goldenberry. The dashed lines represent the critical points of the freezing curve of the center of the sample and the upper magnification represents a specific sample, where the subcooling and initial freezing point are observed.

2022; Struchaiev et al., 2019).

3.2. Differential scanning calorimetry

Figure 6 shows the thermogram of fresh goldenberry pulp (moisture 4.10 ± 0.04 kg_w/kg_T and soluble solids 14.30 ± 0.11° Brix), where both an endothermic behavior and a glass transition are observed. The glass transition temperature range is detailed in Table 1, with the midpoint (T'_g) identified at −35.8 ± 0.2 °C. This T'_g value is close to those reported for other fruits, including Deglet Nour (Guizani et al., 2010), blueberries (Díaz, Henríquez, Enrione, & Matiacevich, 2011; Vásquez, Díaz-Calderón, Enrione, & Matiacevich, 2013), Chinese gooseberries (Wang, Zhang, & Chen, 2008), and raspberries (Syamaladevi, Sablani, Tang, Powers, & Swanson, 2009), which exhibit T'_g values of −42.5, [−44.0 to −40.3], −55.8 and − 62.1 °C, respectively. The variation in T'_g among these matrices is primarily attributed to differences in water content and the molecular weight of solutes (Guizani et al., 2010), since higher moisture content generally leads to lower T'_g values (Collares, Finzer, & Kieckbusch, 2004; Roos, 1993; Roos & Drusch, 2016). In the case of goldenberry, these differences can be further explained by the predominant carbohydrate composition of its cell wall, particularly the presence of sucrose (35 g/100 g total sugars), fructose (29 g/100 g), and glucose (25 g/100 g) (Ramadan & Moersel, 2007). These low molecular weight sugars have been shown to significantly influence T'_g, as evidenced in similar food matrices such as mango (Yamamoto, Fong-in, & Kawai, 2021). Moreover, the T'_g for sucrose, glucose and fructose are −41 °C, −53 °C and − 53 °C respectively (Roos & Drusch, 2016). These values are comparable to the values obtained for goldenberry pulp.

To date, limited research has been conducted on the thermal properties of high Andean berries, particularly regarding the specific heat capacity (c_p) of goldenberry. The specific heat capacity is a critical parameter in heat transfer calculations and plays a key role in the design and optimization of refrigeration, freezing, and cold storage systems, as well as in defining the operational parameters for these processes.

The Table 2 presents the c_p values of fresh goldenberry pulp across different temperature ranges. These values were derived from the thermal profile (Fig. 6) and calculated using Eq. 10. A Statistically significant difference in c_p was observed between temperature ranges ($p <$ 0.05), which may be attributed to variations in moisture and/or water mobility (Farinu & Baik, 2007; Murakonda, Patel, & Dwivedi, 2022). At temperatures above 0 °C, the c_p values obtained for goldenberry pulp were comparable to those reported for other fruits such as murtilla (3.78 kJ/kg·°C), cashew (3.816 kJ/kg·°C), and bael (3.2512 kJ/kg·K). The values for murtilla were determined using differential scanning calorimetry (DSC) (Lemus-Mondaca, Ah-Hen, Vega-Gálvez, & Zura-Bravo, 2016), whereas those for cashew and bael were estimated from proximate composition based on moisture (Singh, Abdullah, Pradhan, & Mishra, 2019; Sonawane, Pathak, & Pradhan, 2020).

Table 1
Glass transition of maximally concentrated sample range. Initial, mean and final temperature of goldenberry pulp T'_g.

T_{gi} (°C)	T_g (°C)	T_{ge} (°C)
−33.9 ± 0.2	−35.8 ± 0.2	−37.7 ± 0.2

Table 2
Specific heat (kJ/kg K) of goldenberry pulp.

≤ T_{ge}	$T_{ge} \leq \leq T_{gi}$	≥ T_{gi}	Fresh *	Fresh **	*p* value
1.988 ± 0.023 ^{d}	2.195 ± 0.096 ^{c}	2.605 ± 0.138 ^{b}	3.975 ± 0.013 ^{a}	3.953 ± 0.021 ^{a}	0.000

Nota. Superscripts of the same letters of the mean c_p values indicate no significant differences according to Tukey's test (pvalue <0.05); (*) heating; (**) cooling.

$$c_p = \frac{q}{m^* \Delta T} \tag{10}$$

In the Table 2 shows, the c_p values of the frozen sample were measured over three distinct periods: the rubbery state, the glass transition, and the glassy state.

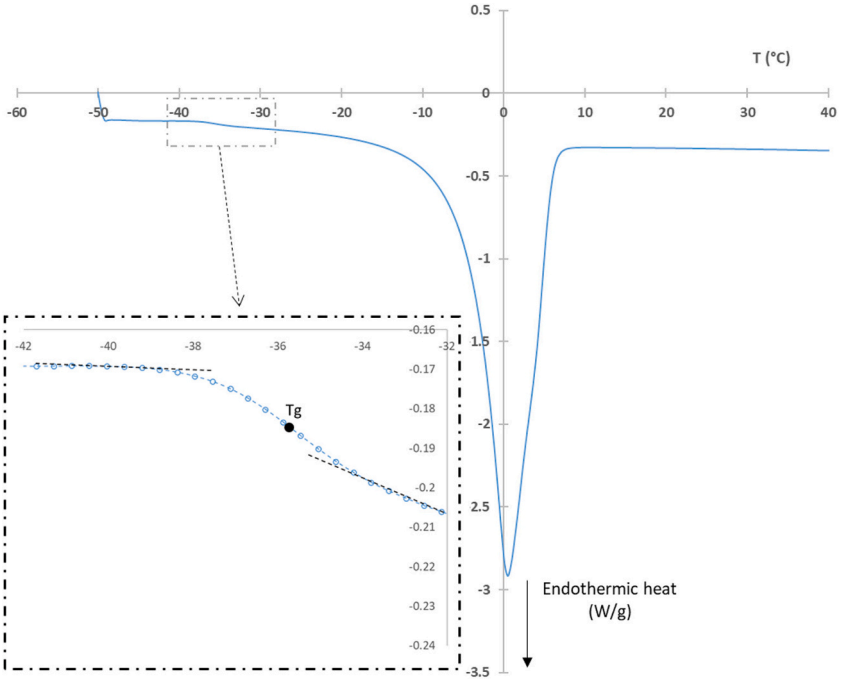

Fig. 6. Thermogram of goldenberry pulp.

3.3. Surface thermal analysis by infrared thermography

In the frozen food industry, accurate recording and monitoring of temperature during the fruit freezing process is critically important, as it ensures both the completeness and uniformity of freezing by promoting thermal equilibrium between the sample and the surrounding freezing air. Infrared (IR) thermography has proven to be an effective non-invasive tool for thermal analysis in a variety of food matrices, including pork (Castro-Giraldez et al., 2014) and fresh potatoes (Cuibus et al., 2014), and has been successfully applied in freezing operations.

To accurately interpret the radiant energy emitted from the fruit surface as photon flux, captured by the pyrosensor of the infrared camera during the freezing process, it is essential to apply a radiative heat transfer model. In this context, the Stefan–Boltzmann law provides the theoretical framework required for such modeling. This model should enable the estimation of the fruit's surface emissivity, the radiative energy received from the surrounding environment, and the energy absorbed by the air layer between the fruit and the infrared camera. (Castro-Giraldez et al., 2014; Cuibus et al., 2014; Tomas-Egea et al., 2022; Traffano-Schiffo et al., 2014). These terms are integrated in Eq. 11.

$$E_T = \varepsilon_C \sigma {T_C}^4 = F{\cdot}\varepsilon_{obj}\sigma T_{obj}^4 + E_{ent} - (1-\tau_{air})F{\cdot}\sigma T_{air}^4 \quad (11)$$

Where E_T is the total energy received by the camera (W/m^2), ε_C is the emissivity set in the thermographic camera ($\varepsilon_C = 1$), σ is the Stefan-Boltzman constant (5.67 × 10^{-8} W/m^{2}K^4), T_C is the temperature obtained by the thermographic camera, F is the geometric factor that can be taken as 1 when the camera is placed perpendicular to the samples, ε_{obj} is the emissivity of the goldenberry, T_{obj} is the surface temperature of the goldenberry, E_{ent} is the energy of the environment on the object obtained with the reference material, τ_{air} is the air permeability which, when it is less than 30 cm from the fruit and the RH of the environment is less than saturation, can be considered equal to 1, leaving this term as zero.

Figure 7 shows the emissivity profile of fresh goldenberry during the freezing process. In the initial cooling phase (0–5 min), a significant decrease in emissivity is observed, from 0.959 ± 0.019 to 0.837 ± 0.002. This reduction may be attributed to surface dehydration of the fruit, likely caused by the low relative humidity conditions within the convective freezer equipped with a no-frost system (Fig. 8). The dehydration phenomenon is driven by a water activity gradient established between the fruit surface and the surrounding air, which promotes the migration of both intracellular and extracellular water to the surface. During the subsequent freezing phase, the emissivity remains relatively stable at approximately 0.845 ± 0.007. This stability is associated with the onset of nucleation and the formation of ice, which induces a chemical potential gradient in the water, leading to both internal and surface ice crystallization (Castro-Giraldez et al., 2014). Concurrently, the surface temperature of the fruit drops rapidly from −4.94 ± 0.17 °C to −28.68 ± 0.12 °C over a 13 min period. Between 18 and 28 min, corresponding to the final stage of the freezing phase, an increase in emissivity is observed from 0.8317 ± 0.003 to 0.93 ± 0.03 (Figs. 7 and 9). This rise may be attributed to the progressive reduction in surface temperature as the fruit approaches thermal equilibrium with the surrounding freezing air. From 28 min until the end of the process, the emissivity of the goldenberry remains stable at approximately 0.9506 ± 0.010. Notably, this stage coincides with the sample reaching its vitrification temperature, recorded at −35.8 ± 0.2 °C (Fig. 9). Similar trends in emissivity variation during freezing processes have been reported in previous studies. Cuibus et al. (2014) and Castro-Giraldez et al. (2014) observed an initial decrease in emissivity, from 0.97 to 0.87 in potatoes and from 0.90 to 0.96 in pork, followed by a subsequent increase after freezing. This behavior aligns with the pattern observed in the present study. In contrast, (Arnoldussen et al., 2022). reported a continuous decline in emissivity during the freezing of sweet cherry reproductive shoots, with values dropping from 0.88 to 0.46 as the temperature decreased from 14 °C to −10 °C.

3.4. Dielectric properties in radiofrequency range

During the freezing process of goldenberry, a progressive decrease in the dielectric constant (log ε') is observed over time and with an increasing angular frequency (log ω) (Fig. 10). The figure shows the exponential stage of α- and β-dispersions, with relaxation frequencies shifting to lower values during freezing. The dielectric constant declines in both cases due to reduced molecular mobility in the liquid phase and in absorbed water, associated with dehydration driven by ice formation., The dielectric spectra in Fig. 10 exhibit a clear β-dispersion (within the 5.5 to 7.5 log(rad/s) during the first 13 min of freezing. This dispersion is attributed to the orientation of fixed charges associated with macromolecules and/or interfacial polarization phenomena, such as the Maxwell–Wagner effect, commonly observed in biological tissues (Albelda Aparisi, Fortes Sanchez, Contat Rodrigo, Masot Peris, & Laguarda-Miro, 2021; Tomas-Egea et al., 2022). The orientation capacity of fixed charges on tissue proteins and carbohydrates is modulated by adsorbed water, and thus, any water-reducing mechanism

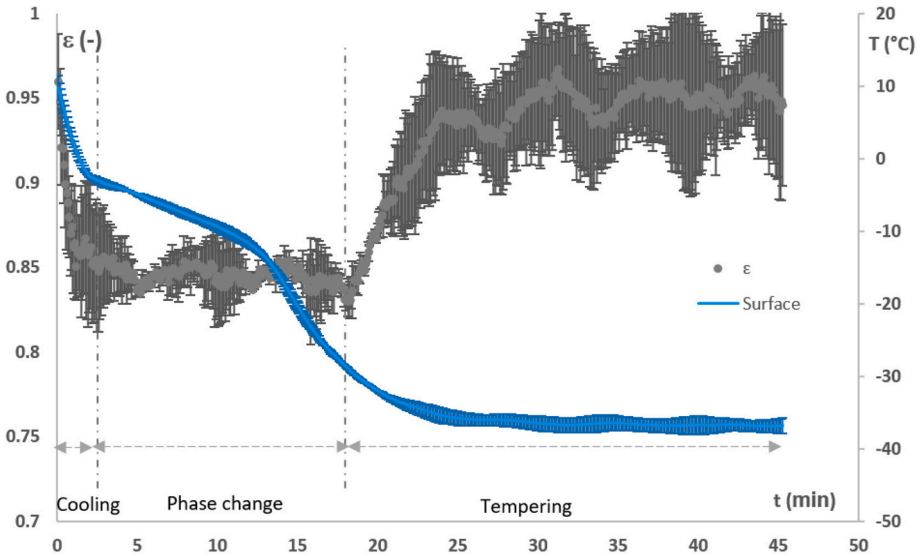

Fig. 7. Kinetics of goldenberry emissivity during the freezing process.

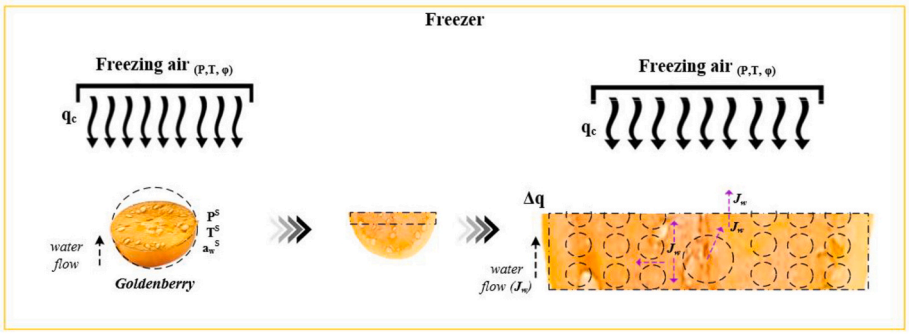

Fig. 8. Thermal analysis and water mobility during freezing of goldenberry.

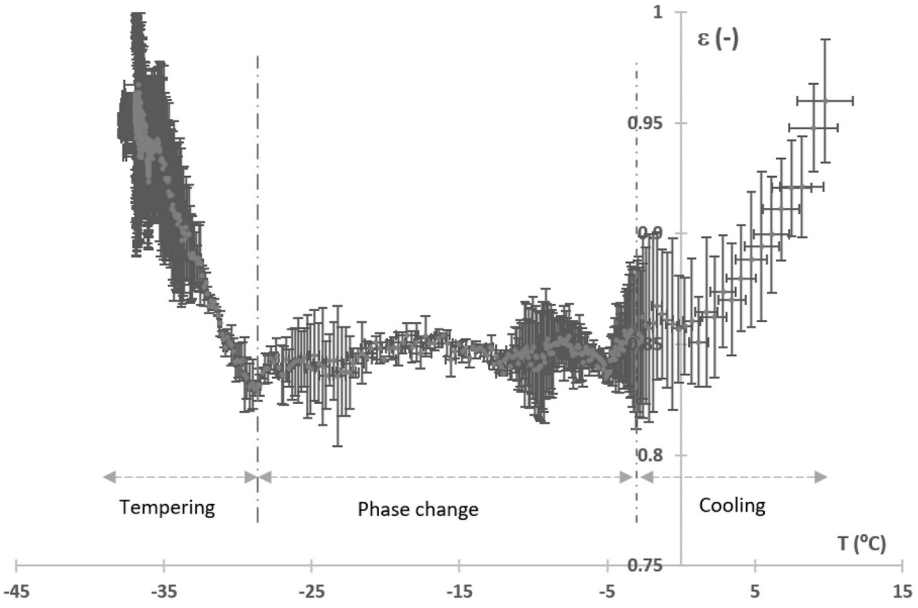

Fig. 9. Emissivity profile of goldenberry as a function of temperature.

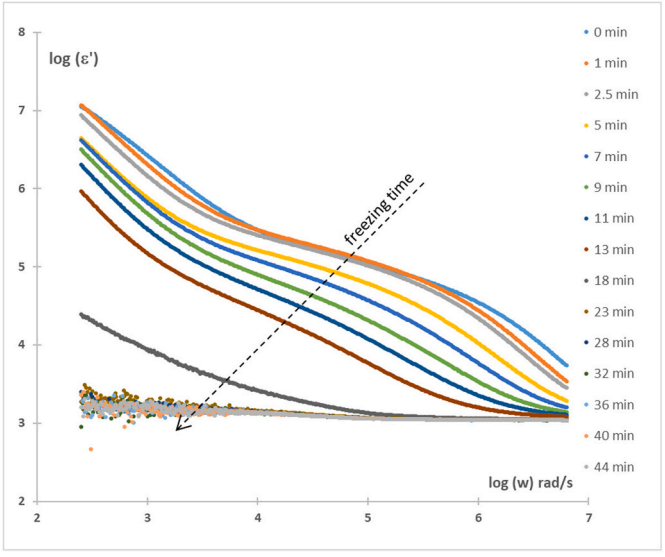

Fig. 10. Evolution of the dielectric spectra of goldenberry during the freezing process.

directly impacts their dielectric behavior. In addition, α-dispersion is also observed, primarily resulting from the orientation of mobile charges. In goldenberry, this mechanism is fundamentally associated with native ions of the fruit (Kuang & Nelson, 1998). From minute 18 until the end of the freezing process, the ε' values continue to decrease, reaching a stabilization phase. This behavior is consistent with the reduced ability of biological materials to store electrical energy as a result of decreased water mobility and availability during the liquid–solid phase transition (Heileman et al., 2013). Such limitations hinder the detection of dielectric spectra, as previously described in studies on frozen biological matrices (Alexander, Shaw, & Muckenhirn, 1937; Auty & Cole, 1952; Pandey, Vandermeiren, Dimiccoli, & Stiens, 2018; Zhang, Shen, & Luo, 2010).

Our findings align with prior observations reported by Arteaga et al. (2021) in the monitoring of blueberry freezing, and by Tomas-Egea et al. (2022), who used radiofrequency spectrophotometry to determine the critical freezing point of chicken meat. In both cases, a consistent decrease in ε' values was reported across different frequencies and freezing durations, a trend similarly observed in our study.

3.5. *Kinetics of α and β dispersions*

To identify the critical points of the goldenberry freezing process and to elucidate the influence of tissue structure and chemical composition on photon flux, it is essential to analyze α- and β-relaxations using Eqs. 5

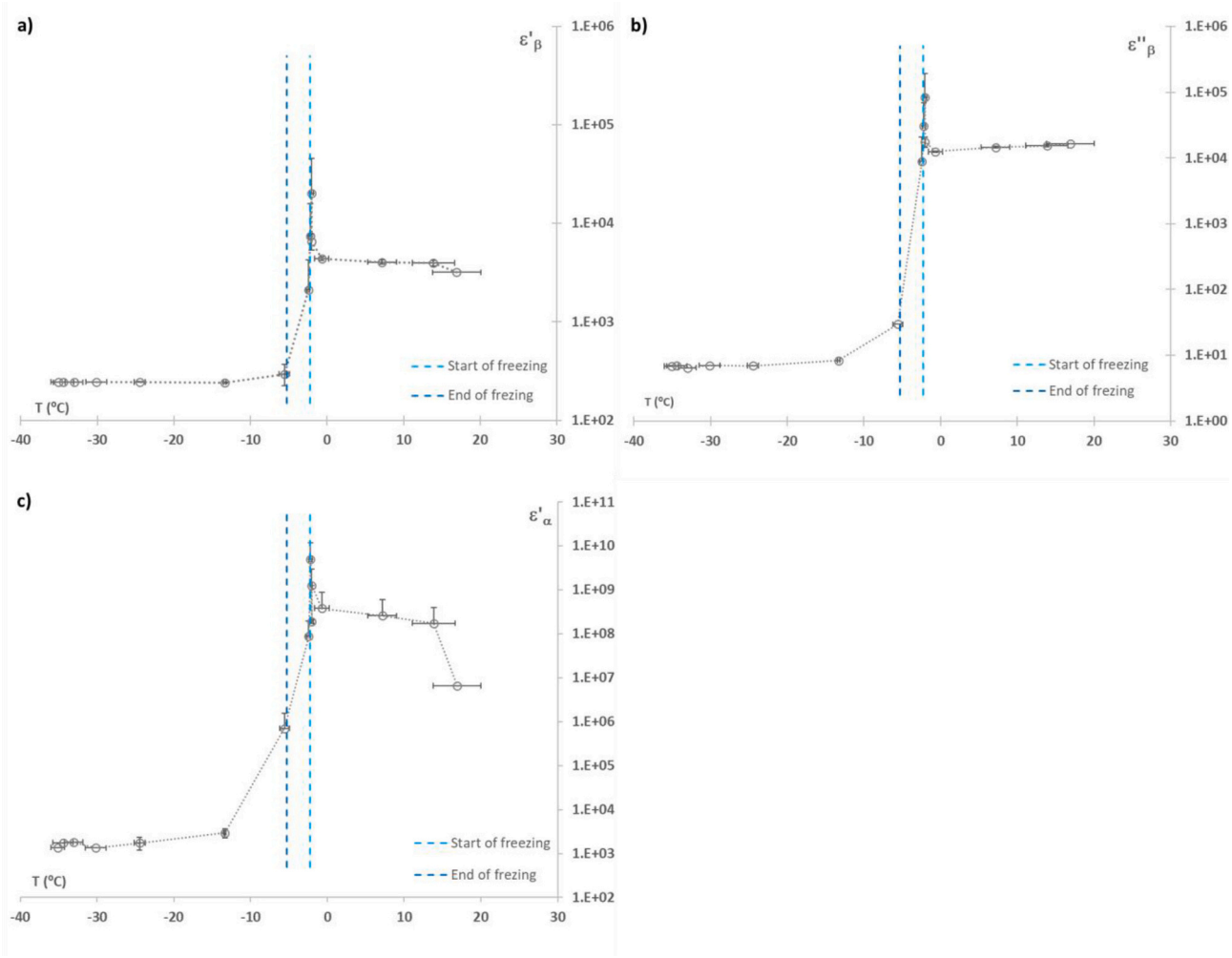

Fig. 11. Dielectric properties with respect to internal temperature, where a) dielectric constant in β relaxation, b) dielectric loss factor in β relaxation and c) dielectric constant in α relaxation.

and 6. Fig. 11 illustrates these critical transitions, consistent with descriptions by Fan and Roos (2017) and Roos (2010). Specifically, the onset of freezing can be inferred from the maximum of the real part of the dielectric constant (ε') within the β-dispersion region, as shown in Fig. 11(a). This behavior is associated with the high surface tension of agglomerated ice cristal Ih, which produces a high Maxwell Wagner effect, allowing to detect the initial ice crystal formation (Agranovich, Ben Ishai, Katz, Bezman, & Feldman, 2016; Cuibus et al., 2014; Tomas-Egea et al., 2022). A similar trend is observed in the α-dispersion region (Fig. 11(c)), where a sharp increase in ε' is attributed to the ionic concentration. In goldenberry tissue, the liquid phase is rich in electrolytes and sugars; as ice crystals form, cryoconcentration initially increases electrolyte concentration, amplifying the α-dispersion response. However, upon reaching saturation and supersaturation, the exponential rise in viscosity restricts ionic mobility, thereby diminishing the α-dispersion effect (Bittelli, Flury, & Roth, 2004; Fan & Roos, 2017; Kono, Imamura, & Nakagawa, 2021; Sasaki et al., 2017). The final freezing point can also be clearly determined. As demonstrated in Fig. 11(c), corresponding to α-dispersion, ε'exhibits a pronounced trend change around −5.27 °C, marking the completion of ice crystal formation. This trend is also corroborated by Fig. 11(b), which shows the loss factor (ε") in the β-dispersion region. A progressive decline in ε" is observed after the maximum peak, indicating a diminished ability of the system to dissipate energy due to increased rigidity of the frozen matrix (Roos, 2010; Talja & Roos, 2001; Tomas-Egea et al., 2022).

During the freezing process, initial ice nuclei typically form at the fruit surface. This induces surface dehydration and creates a gradient in the water chemical potential, which drives water migration from the interior toward the surface. Under atmospheric pressure conditions, the formation of ice Ih crystals is favored. These crystals exhibit high surface tension, which further attracts nearby liquid water molecules, promoting the growth of agglomerated ice structures. As a result, water is simultaneously attracted to the surface and to nucleation centers, leading to high water mobility throughout the freezing process.

3.6. *Water mobility role*

The location of ice nucleation plays a critical role in the extent of cellular damage. When ice nucleation occurs extracellularly (in the apoplastic space), water is drawn out of the cells, and the resulting ice crystal growth tends to cause minimal structural disruption. In contrast, intracellular nucleation (e.g., within the vacuole) leads to expansion and rupture of cell membranes, significantly increasing tissue damage.

In our study, changes in surface emissivity were associated with dehydration and water migration dynamics, while dielectric α-dispersion reflected alterations in ionic mobility, likely due to membrane disruption and solute concentration changes. β-dispersion, on the other hand, captured interfacial polarization effects related to ice crystal growth and macromolecular rearrangements. Together, these thermal and dielectric parameters provide a non-invasive means of assessing structural changes during freezing, offering valuable information for optimizing processing protocols.

4. Conclusions

The findings indicate that infrared thermography is a viable method for monitoring the freezing process of goldenberry, as it facilitates the observation of surface temperature variations. This tool facilitates the identification of critical points in the process, such as the glass transition, from the estimation of the emissivity at different stages of freezing; supercooling stage: Detected by a continuous temperature drop without phase change, and a sharp decrease in emissivity from ~0.959 to 0.837. This stage ends with the onset of nucleation. Ice nucleation and crystallization stage: Identified by a plateau or slight rebound in temperature due to latent heat release, along with stable emissivity (~0.845) and changes in dielectric α- and β-dispersions, reflecting structural changes (β) and cryoconcentration (α). And finally, Vitrification stage: Occurs after ice crystallization is completed. Emissivity increases again (~0.93 to 0.951) as the system approaches the glass transition. The glass transition temperature (−35.8 °C) marks the point where molecular mobility becomes severely restricted, thus preserving cellular structure by preventing further ice growth and solute migration. This enhances long-term structural and biochemical stability during frozen storage.

Conversely, the utilization of sensors founded upon radiofrequency spectrophotometry facilitates the acquisition of not merely surface information, as is the case in thermography, but also the internal properties of samples undergoing the freezing process. This is imperative for the precise detection of the critical points of the process (melting point and glass transition), thereby ensuring uniform and efficient freezing of the goldenberry.

CRediT authorship contribution statement

T. Chuquizuta: Writing – original draft, Software, Investigation, Formal analysis, Data curation. **W. Castro:** Writing – review & editing, Visualization, Supervision, Data curation, Conceptualization. **M. Castro-Giraldez:** Writing – review & editing, Visualization, Validation, Supervision, Funding acquisition, Formal analysis, Data curation, Conceptualization. **P.J. Fito:** Writing – review & editing, Visualization, Validation, Supervision, Resources, Funding acquisition, Formal analysis, Data curation, Conceptualization.

Funding

Funding for open access charge: Universitat Politècnica de València.

Declaration of competing interest

The authors declare that they have no known competing financial interests or personal relationships that could have appeared to influence the work reported in this paper.

The authors declare the following financial interests/personal relationships which may be considered as potential competing interests:

Marta Castro-Giraldez reports financial support was provided by Polytechnic University of Valencia. Marta Castro-Giraldez reports a relationship with Polytechnic University of Valencia that includes: board membership. If there are other authors, they declare that they have no known competing financial interests or personal relationships that could have appeared to influence the work reported in this paper.

Acknowledgment

Funding for open access charge: Universitat Politècnica de València.

Data availability

Data will be made available on request.

References

Agranovich, D., Ben Ishai, P., Katz, G., Bezman, D., & Feldman, Y. (2016). Dielectric spectroscopy study of water dynamics in frozen bovine milk. *Colloids and Surfaces B: Biointerfaces, 141*, 390–396. https://doi.org/10.1016/j.colsurfb.2016.01.031

Albelda Aparisi, P., Fortes Sanchez, E., Contat Rodrigo, L., Masot Peris, R., & Laguarda-Miro, N. (2021). A rapid electrochemical impedance spectroscopy and sensor-based method for monitoring freeze-damage in tangerines. *IEEE Sensors Journal, 21*(10), 12009–12018. https://doi.org/10.1109/JSEN.2021.3065846

Alexander, L. T., Shaw, T. M., & Muckenhirn, R. J. (1937). Detection of freezing point by dielectric measurements. *Soil Science Society of America Journal, 1*(C), 113–119. https://doi.org/10.2136/sssaj1937.03615995000100000014x

Arnoldussen, B., Alhamid, J., Wang, P., Mo, C., Zhang, X., Zhang, Q., & Whiting, M. (2022). Internal freezing and heat loss of apple (Malus domestica Borkh.) and sweet cherry (Prunus avium L.) reproductive buds are decreased with cellulose nanocrystal dispersions. *Frontiers in Plant Science, 13*. https://doi.org/10.3389/fpls.2022.949537

Arteaga, H., Robleto-Martinez, E., de Sousa, C., Silva, A., Souto, S., Batista, J., & Xavier Costa, E. J. (2021). Postharvest freezing process assessment of the blueberry structure in three acts: Bioimpedance, color, and granulometry analysis. *LWT, 151*, Article 112237. https://doi.org/10.1016/j.lwt.2021.112237

Auleda, J. M., Raventós, M., Sánchez, J., & Hernández, E. (2011). Estimation of the freezing point of concentrated fruit juices for application in freeze concentration. *Journal of Food Engineering, 105*(2), 289–294. https://doi.org/10.1016/j.jfoodeng.2011.02.035

Auty, R. P., & Cole, R. H. (1952). Dielectric properties of ice and solid D2O. *The Journal of Chemical Physics, 20*(8), 1309–1314. https://doi.org/10.1063/1.1700726

Balaguera-López, H. E., Espinal-Ruiz, M., Zacarías, L., & Herrera, A. O. (2017). Effect of ethylene and 1-methylcyclopropene on the postharvest behavior of cape gooseberry fruits (*Physalis peruviana* L.). *Food Science and Technology International, 23*(1), 86–96. https://doi.org/10.1177/1082013216658581

Ben Haj Said, L., Bellagha, S., & Allaf, K. (2016). Dehydrofreezing of apple fruits: Freezing profiles, freezing characteristics, and texture variation. *Food and Bioprocess Technology, 9*(2), 252–261. https://doi.org/10.1007/s11947-015-1619-4

Bittelli, M., Flury, M., & Roth, K. (2004). Use of dielectric spectroscopy to estimate ice content in frozen porous media. *Water Resources Research, 40*(4). https://doi.org/10.1029/2003WR002343

Castro-Giraldez, M., Balaguer, N., Hinarejos, E., & Fito, P. J. (2014). Thermodynamic approach of meat freezing process. *Innovative Food Science & Emerging Technologies, 23*, 138–145. https://doi.org/10.1016/j.ifset.2014.03.007

Chandra Roychoudhuri, A. F. K. K. C. (2017). In B. J. Thompson (Ed.), *The nature of light what is a photon?*. CRC Press.

Chi Khang, V., Le Dang, T., Van Muoi, N., & Thanh Truc, T. (2022). Evaluation of freezing temperatures and ripeness levels on the quality characteristics of frozen pineapple fruits. *Journal of Microbiology, Biotechnology and Food Sciences, 12*(3), Article e5439. https://doi.org/10.55251/jmbfs.5439

Chuquizuta, T., Colunche, Y., Rubio, M., Oblitas, J., Arteaga, H., & Castro, W. (2022). Prediction of quality attributes of fresh unpasteurized milk using dielectric spectroscopy coupled to chemometric tools. *Photonics & Electromagnetics Research Symposium (PIERS), 2022*, 776–782. https://doi.org/10.1109/PIERS55526.2022.9792687

Collares, F. P., Finzer, J. R. D., & Kieckbusch, T. G. (2004). Glass transition control of the detachment of food pastes dried over glass plates. *Journal of Food Engineering, 61*(2), 261–267. https://doi.org/10.1016/S0260-8774(03)00098-0

Cuibus, L., Castro-Giraldez, M., Fito, P. J., & Fabbri, A. (2014). Application of infrared thermography and dielectric spectroscopy for controlling freezing process of raw potato. *Innovative Food Science & Emerging Technologies, 24*, 80–87. https://doi.org/10.1016/j.ifset.2013.11.007

Da Silva, D. L., Silveira, A. S., Ronzoni, A. F., & Hermes, C. J. L. (2022). Effect of freezing rate on the quality of frozen strawberries (Fragaria x ananassa). *International Journal of Refrigeration, 144*, 46–54. https://doi.org/10.1016/j.ijrefrig.2022.07.006

De Ancos, B., Sánchez-Moreno, C., De Pascual-Teresa, S., & Cano, M. P. (2012). Freezing preservation of fruits. In *Handbook of fruits and fruit processing* (pp. 103–119). Wiley. https://doi.org/10.1002/9781118352533.ch7.

Delgado, A. E., & Sun, D.-W. (2001). Heat and mass transfer models for predicting freezing processes – A review. *Journal of Food Engineering, 47*(3), 157–174. https://doi.org/10.1016/S0260-8774(00)00112-6

Díaz, P., Henríquez, O., Enrione, J., & Matiacevich, S. (2011). Thermal transitions of pulp and cuticle of blueberries. *Thermochimica Acta, 525*(1–2), 56–61. https://doi.org/10.1016/j.tca.2011.07.021

Fan, F., & Roos, Y. H. (2017). Glass transition-associated structural relaxations and applications of relaxation times in amorphous food solids: A review. *Food Engineering Reviews, 9*(4), 257–270. https://doi.org/10.1007/s12393-017-9166-6

Farinu, A., & Baik, O.-D. (2007). Thermal properties of sweet potato with its moisture content and temperature. *International Journal of Food Properties, 10*(4), 703–719. https://doi.org/10.1080/10942910601137482

Gallego, B., Verdú, J. R., Carrascal, L. M., & Lobo, J. M. (2016). A protocol for analysing thermal stress in insects using infrared thermography. *Journal of Thermal Biology, 56*, 113–121. https://doi.org/10.1016/j.jtherbio.2015.12.006

Gonçalves, B. J., Giarola, T. M.d. O., Pereira, D. F., Vilas Boas, E. V.d. B., & de Resende, J. V. (2016). Using infrared thermography to evaluate the injuries of cold-stored guava. *Journal of Food Science and Technology, 53*(2), 1063–1070. https://doi.org/10.1007/s13197-015-2141-4

Gonçalves, B. J., Lago, A. M. T., Machado, A. A., Giarola, T. M.d. O., Prado, M. E. T., & de Resende, J. V. (2018). Infrared (IR) thermography applied in the freeze-drying of gelatin model solutions added with ethanol and carrier agents. *Journal of Food Engineering, 221*, 77–87. https://doi.org/10.1016/j.jfoodeng.2017.10.004

Guizani, N., Al-Saidi, G. S., Rahman, M. S., Bornaz, S., & Al-Alawi, A. A. (2010). State diagram of dates: Glass transition, freezing curve and maximal-freeze-concentration condition. *Journal of Food Engineering, 99*(1), 92–97. https://doi.org/10.1016/j.jfoodeng.2010.02.003

Guo, W., Fang, L., Liu, D., & Wang, Z. (2015). Determination of soluble solids content and firmness of pears during ripening by using dielectric spectroscopy. *Computers and Electronics in Agriculture, 117*, 226–233. https://doi.org/10.1016/j.compag.2015.08.012

Hajji, W., Gliguem, H., Bellagha, S., & Allaf, K. (2022). Structural and textural improvements of strawberry fruits by partial water removal prior to conventional freezing process. *Journal of Food Measurement and Characterization, 16*(5), 3344–3353. https://doi.org/10.1007/s11694-022-01443-w

Harrap, M. J. M., Hempel de Ibarra, N., Whitney, H. M., & Rands, S. A. (2018). Reporting of thermography parameters in biology: A systematic review of thermal imaging literature. *Royal Society Open Science, 5*(12), Article 181281. https://doi.org/10.1098/rsos.181281

Heileman, K., Daoud, J., & Tabrizian, M. (2013). Dielectric spectroscopy as a viable biosensing tool for cell and tissue characterization and analysis. *Biosensors and Bioelectronics, 49*, 348–359. https://doi.org/10.1016/j.bios.2013.04.017

Kono, S., Imamura, H., & Nakagawa, K. (2021). Non-destructive monitoring of food freezing process by microwave resonance spectroscopy with an open-ended coaxial resonator. *Journal of Food Engineering, 292*, Article 110293. https://doi.org/10.1016/j.jfoodeng.2020.110293

Kuang, W., & Nelson, S. O. (1998). Low-frequency dielectric properties of biological tissues: A review with some new insights. *Transactions of ASAE, 41*(1), 173–184. https://doi.org/10.13031/2013.17142

Lan, W., Hui, X., Nicolaï, B., Verboven, P., Qin, J., Renard, C. M. G. C., … Pan, L. (2024). Visualizing the structural and chemical heterogeneity of fruit and vegetables using advanced imaging techniques: Fundamentals, instrumental aspects, applications and future perspectives. *Critical Reviews in Food Science and Nutrition*. https://doi.org/10.1080/10408398.2024.2384650

Lemus-Mondaca, R., Ah-Hen, K., Vega-Gálvez, A., & Zura-Bravo, L. (2016). Effect of high hydrostatic pressure on rheological and thermophysical properties of murtilla (Ugni molinae Turcz) berries. *Journal of Food Science and Technology, 53*(6), 2725–2732. https://doi.org/10.1007/s13197-016-2244-6

Li, H.-C., Cheng, H.-P., & Cheng, C.-C. (2025). Shelf temperature estimation of a vacuum freeze dryer by infrared thermal imaging camera. *Quantitative InfraRed Thermography Journal, 1–16*. https://doi.org/10.1080/17686733.2025.2463264

Liu, D., & Guo, W. (2017). Nondestructive determination of soluble solids content of persimmons by using dielectric spectroscopy. *International Journal of Food Properties, 20*(sup3), S2596–S2611. https://doi.org/10.1080/10942912.2017.1381114

Loayza-Salazar, S., Siche, R., Vegas, C., Chávez-Llerena, R. T., Encina-Zelada, C. R., Calla-Florez, M., & Comettant-Rabanal, R. (2024). Novel Technologies in the Freezing Process and Their Impact on the quality of fruits and vegetables. *Food Engineering Reviews, 16*(3), 371–395. https://doi.org/10.1007/s12393-024-09371-9

Lopez, H. E. B., Fischer, G., & Magnitskiy, S. (2024). Physiology and biochemistry of the Physalis peruviana fruit. In *Handbook of Goldenberry (Physalis Peruviana)* (pp. 121–137). Elsevier. https://doi.org/10.1016/B978-0-443-15433-1.00011-X.

Murakonda, S., Patel, G., & Dwivedi, M. (2022). Characterization of engineering properties and modeling mass and fruit fraction of wood apple (Limonia acidissima) fruit for post-harvest processing. *Journal of the Saudi Society of Agricultural Sciences, 21*(4), 267–277. https://doi.org/10.1016/j.jssas.2021.09.005

Ojha, K. S., Kerry, J. P., Tiwari, B. K., & O'Donnell, C. (2016). Freezing for food preservation. In *Reference module in food science*. Elsevier. https://doi.org/10.1016/B978-0-08-100596-5.03108-5.

Olivares-Tenorio, M.-L., Dekker, M., Verkerk, R., & van Boekel, M. A. J. S. (2016). Health-promoting compounds in cape gooseberry (Physalis peruviana L.): Review from a supply chain perspective. *Trends in Food Science & Technology, 57*, 83–92. https://doi.org/10.1016/j.tifs.2016.09.009

Ozcelik, M. M., Ozcelik, A., Aksu, M., & Ozkan, G. (2024). Postharvest technology and packing of Physalis peruviana. In *Handbook of Goldenberry (Physalis Peruviana)* (pp. 291–298). Elsevier. https://doi.org/10.1016/B978-0-443-15433-1.00031-5.

Pandey, G., Vandermeiren, W., Dimiccoli, L., & Stiens, J. (2018). Contactless monitoring of food drying and freezing processes with millimeter waves. *Journal of Food Engineering, 226*, 1–8. https://doi.org/10.1016/j.jfoodeng.2018.01.003

Poirier-Pocovi, M., Volder, A., & Bailey, B. N. (2020). Modeling of reference temperatures for calculating crop water stress indices from infrared thermography. *Agricultural Water Management, 233*, Article 106070. https://doi.org/10.1016/j.agwat.2020.106070

Puente, L., Vega-Gálvez, A., Fuentes, I., Stucken, K., Rodríguez, A., & Pastén, A. (2021). Effects of drying methods on the characterization of fatty acids, bioactive compounds and antioxidant capacity in a thin layer of physalis (Physalis peruviana L.) pulp. *Journal of Food Science and Technology, 58*(4), 1470–1479. https://doi.org/10.1007/s13197-020-04659-0

Puente, L. A., Pinto-Muñoz, C. A., Castro, E. S., & Cortés, M. (2011). Physalis peruviana Linnaeus, the multiple properties of a highly functional fruit: A review. *Food Research International, 44*(7), 1733–1740. https://doi.org/10.1016/j.foodres.2010.09.034

Ramadan, M. F., & Moersel, J. T. (2007). Impact of enzymatic treatment on chemical composition, physicochemical properties and radical scavenging activity of goldenberry (*Physalis peruviana* L.) juice. *Journal of the Science of Food and Agriculture, 87*(3), 452–460. https://doi.org/10.1002/jsfa.2728

Roos, Y. H. (1993). Water activity and physical state effects on amorphous food stability. *Journal of Food Processing and Preservation, 16*(6), 433–447. https://doi.org/10.1111/j.1745-4549.1993.tb00221.x

Roos, Y. H. (2010). Glass transition temperature and its relevance in food processing. *Annual Review of Food Science and Technology, 1*(1), 469–496. https://doi.org/10.1146/annurev.food.102308.124139

Roos, Y. H., & Drusch, S. (2016). Food components and polymers. In *Phase transitions in foods* (pp. 115–172). Elsevier. https://doi.org/10.1016/B978-0-12-408086-7.00005-X.

Sasaki, K., Panagopoulou, A., Kita, R., Shinyashiki, N., Yagihara, S., Kyritsis, A., & Pissis, P. (2017). Dynamics of uncrystallized water, ice, and hydrated protein in partially crystallized gelatin–water mixtures studied by broadband dielectric spectroscopy. *The Journal of Physical Chemistry B, 121*(1), 265–272. https://doi.org/10.1021/acs.jpcb.6b04756

Shammi, S., Sohel, F., Diepeveen, D., Zander, S., & Jones, M. G. K. (2023). Machine learning-based detection of frost events in wheat plants from infrared thermography. *European Journal of Agronomy, 149*, Article 126900. https://doi.org/10.1016/j.eja.2023.126900

Shammi, S., Sohel, F., Diepeveen, D., Zander, S., Jones, M. G. K., Bekuma, A., & Biddulph, B. (2022). Machine learning-based detection of freezing events using infrared thermography. *Computers and Electronics in Agriculture, 198*, Article 107013. https://doi.org/10.1016/j.compag.2022.107013

Singh, S. S., Abdullah, S., Pradhan, R. C., & Mishra, S. (2019). Physical, chemical, textural, and thermal properties of cashew apple fruit. *Journal of Food Process Engineering, 42*(5). https://doi.org/10.1111/jfpe.13094

Sonawane, A., Pathak, S. S., & Pradhan, R. C. (2020). Physical, thermal, and mechanical properties of bael fruit. *Journal of Food Process Engineering, 43*(6). https://doi.org/10.1111/jfpe.13393

Struchaiev, N., Postol, Y., Stopin, Y., & Borokhov, I. (2019). Determination of the duration of spherical-shaped berries freezing under the conditions stationary heat flow. In *Modern development paths of agricultural production* (pp. 405–414). Springer International Publishing. https://doi.org/10.1007/978-3-030-14918-5_42.

Syamaladevi, R. M., Sablani, S. S., Tang, J., Powers, J., & Swanson, B. G. (2009). State diagram and water adsorption isotherm of raspberry (Rubus idaeus). *Journal of Food Engineering, 91*(3), 460–467. https://doi.org/10.1016/j.jfoodeng.2008.09.025

Talja, R. A., & Roos, Y. H. (2001). Phase and state transition effects on dielectric, mechanical, and thermal properties of polyols. *Thermochimica Acta, 380*(2), 109–121. https://doi.org/10.1016/S0040-6031(01)00664-5

Tomas-Egea, J. A., Castro-Giraldez, M., Colom, R. J., & Fito, P. J. (2022). New technique for determining the critical freezing temperatures of chicken breast based on radiofrequency photospectrometry. *Journal of Food Engineering, 333*, Article 111155. https://doi.org/10.1016/j.jfoodeng.2022.111155

Tomas-Egea, J. A., Traffano-Schiffo, M. V., Castro-Giraldez, M., & Fito, P. J. (2021). Hot air and microwave combined drying of potato monitored by infrared thermography. *Applied Sciences, 11*(4), 1730. https://doi.org/10.3390/app11041730

Traffano-Schiffo, M. V., Castro-Giraldez, M., Colom, R. J., & Fito, P. J. (2018). Innovative photonic system in radiofrequency and microwave range to determine chicken meat quality. *Journal of Food Engineering, 239*, 1–7. https://doi.org/10.1016/j.jfoodeng.2018.06.029

Traffano-Schiffo, M. V., Castro-Giraldez, M., Colom, R. J., Talens, P., & Fito, P. J. (2021). New methodology to analyze the dielectric properties in radiofrequency and microwave ranges in chicken meat during postmortem time. *Journal of Food Engineering, 292*, Article 110350. https://doi.org/10.1016/j.jfoodeng.2020.110350

Traffano-Schiffo, M. V., Castro-Giraldez, M., Fito, P. J., & Balaguer, N. (2014). Thermodynamic model of meat drying by infrarred thermography. *Journal of Food Engineering, 128*, 103–110. https://doi.org/10.1016/j.jfoodeng.2013.12.024

Usamentiaga, R., Venegas, P., Guerediaga, J., Vega, L., Molleda, J., & Bulnes, F. (2014). Infrared thermography for temperature measurement and non-destructive testing. *Sensors, 14*(7), 12305–12348. https://doi.org/10.3390/s140712305

Vasco, C., Ruales, J., & Kamal-Eldin, A. (2008). Total phenolic compounds and antioxidant capacities of major fruits from Ecuador. *Food Chemistry, 111*(4), 816–823. https://doi.org/10.1016/j.foodchem.2008.04.054

Vásquez, C., Díaz-Calderón, P., Enrione, J., & Matiacevich, S. (2013). State diagram, sorption isotherm and color of blueberries as a function of water content. *Thermochimica Acta, 570*, 8–15. https://doi.org/10.1016/j.tca.2013.07.029

Vega-Gálvez, A., López, J., Ah-Hen, K., Torres, M., & Lemus-Mondaca, R. (2014). Thermodynamic properties, sorption isotherms and glass transition temperature of cape gooseberry (Physalis peruviana L.). *Food Technology and Biotechnology, 52*(1), 83–92.

Wang, H., Zhang, S., & Chen, G. (2008). Glass transition and state diagram for fresh and freeze-dried Chinese gooseberry. *Journal of Food Engineering, 84*(2), 307–312. https://doi.org/10.1016/j.jfoodeng.2007.05.024

Wang, Z., Ding, F., Ge, Y., Wang, M., Zuo, C., Song, J., Tu, K., Lan, W., & Pan, L. (2024). Comparing visible and near infrared 'point' spectroscopy and hyperspectral imaging techniques to visualize the variability of apple firmness. *Spectrochimica Acta Part A: Molecular and Biomolecular Spectroscopy, 316*, Article 124344. https://doi.org/10.1016/j.saa.2024.124344

Yamamoto, Y., Fong-in, S., & Kawai, K. (2021). Optimum physical properties of fruit puree for freeze-drying: Effect of pulp content on freeze-concentrated glass transition temperature and yield stress of mango puree. *Journal of Food Engineering, 307*, Article 110649. https://doi.org/10.1016/j.jfoodeng.2021.110649

Zhang, L., Shen, H., & Luo, Y. (2010). Study on the electric conduction properties of fresh and frozen–thawed grass carp (*Ctenopharyngodon idellus*) and tilapia(*Oreochromis niloticus*). *International Journal of Food Science & Technology, 45*(12), 2560–2564. https://doi.org/10.1111/j.1365-2621.2010.02428.x